

Erosion rates and mechanisms of knickzone retreat inferred from ^{10}Be measured across strong climate gradients on the northern and central Andes Western Escarpment

Luca M. Abbühl,¹ Kevin P. Norton,^{1*} John D. Jansen,² Fritz Schlunegger,¹ Ala Aldahan^{3,4} and Göran Possnert⁵

¹ Institute of Geological Sciences, University of Bern, CH-3012 Bern, Switzerland

² Department of Physical Geography and Quaternary Geology, Stockholm University, SE-106 91 Stockholm, Sweden

³ Department of Earth Sciences, Uppsala University, SE-752 36 Uppsala, Sweden

⁴ Department of Geology, United Arab Emirates University, Al Ain, United Arab Emirates

⁵ Tandem Laboratory, Uppsala University, SE-751 20 Uppsala, Sweden

Received 2 September 2010; Revised 10 March 2011; Accepted 14 March 2011

*Correspondence to: Kevin P. Norton, Institute of Geological Sciences, University of Bern, CH-3012 Bern, Switzerland. E-mail: norton@geo.unibe.ch

ESPL

Earth Surface Processes and Landforms

ABSTRACT: A steep escarpment edge, deep gorges and distinct knickzones in river profiles characterize the landscape on the Western Escarpment of the Andes between $\sim 5^\circ\text{S}$ and $\sim 18^\circ\text{S}$ (northern Peru to northern Chile). Strong north–south and east–west precipitation gradients are exploited in order to determine how climate affects denudation rates in three river basins spanning an otherwise relatively uniform geologic and geomorphologic setting. Late Miocene tectonics uplifted the Meseta/Altiplano plateau (~ 3000 m a.s.l.), which is underlain by a series of Tertiary volcanic–volcanoclastic rocks. Streams on this plateau remain graded to the Late Miocene base level. Below the rim of the Meseta, streams have responded to this ramp uplift by incising deeply into fractured Mesozoic rocks via a series of steep, headward retreating knickzones that grade to the present-day base level defined by the Pacific Ocean.

It is found that the Tertiary units on the plateau function as cap-rocks, which aid in the parallel retreat of the sharp escarpment edge and upper knickzone tips. ^{10}Be -derived catchment denudation rates of the Rio Piura (5°S), Rio Pisco (13°S) and Rio Lluta (18°S) average ~ 10 mm ky^{-1} on the Meseta/Altiplano, irrespective of precipitation rates; whereas, downstream of the escarpment edge, denudation rates range from 10 mm ky^{-1} to 250 mm ky^{-1} and correlate positively with precipitation rates, but show no strong correlation with hillslope angles or channel steepness. These relationships are explained by the presence of a cap-rock and climate-driven fluvial incision that steepens hillslopes to near-threshold conditions.

Since escarpment retreat and the precipitation pattern were established at least in the Miocene, it is speculated that the present-day distribution of morphology and denudation rates has probably remained largely unchanged during the past several millions of years as the knickzones have propagated headward into the plateau. Copyright © 2011 John Wiley & Sons, Ltd.

Introduction

One of the most prominent features on the Western Escarpment of the Andes is the distinct escarpment edge delineating the western boundary of the >4000 m a.s.l. Andean plateau (known as the Meseta or Altiplano). Downstream of the plateau, the rivers have formed spectacular valleys, some of which are >1 km deep, due to incision beginning 7.5–8 Ma (von Rotz *et al.*, 2005), or 9–10 Ma (García and Hérial, 2005; Kober *et al.*, 2006; Schildgen *et al.*, 2007, 2010; Thouret *et al.*, 2007; Farías *et al.*, 2008) in response to surface uplift. Valley dissection has proceeded upstream by parallel retreat through headward erosion (Schlunegger *et al.*, 2006), with present-day incision focused in knickzone reaches (García and Hérial, 2005; Hoke *et al.*, 2007; Schildgen *et al.*, 2007). Ignimbrites and volcanoclastic rocks define the uppermost boundaries

of the knickzones at the escarpment edge in all the study basins (Figure 1). At present, the knickzones are located at ~ 40 – 140 km distance from the coast depending on the size of the drainage basin, and whether or not the Coastal Cordillera is submerged (Wipf, 2006). Further studies in northern Chile have shown that the knickzones marking the escarpment edge have evolved at rates ranging from 3 to 6 cm yr^{-1} (Schlunegger *et al.*, 2006). Knickpoint retreat is responsible for vertical incision of deep and narrow gorges at rates of 0.2 mm yr^{-1} in northern Chile (Schlunegger *et al.*, 2006), and 0.4 mm yr^{-1} in central Peru (Schildgen *et al.*, 2007), while incision rates upstream of the knickzones have remained very low, apparently unaffected by the Miocene surface uplift (Schlunegger *et al.*, 2006).

Parallel retreat of knickzones requires the maintenance of a steep headwall during headward migration whereby the rate of removal of material from the base of the slope and that at the

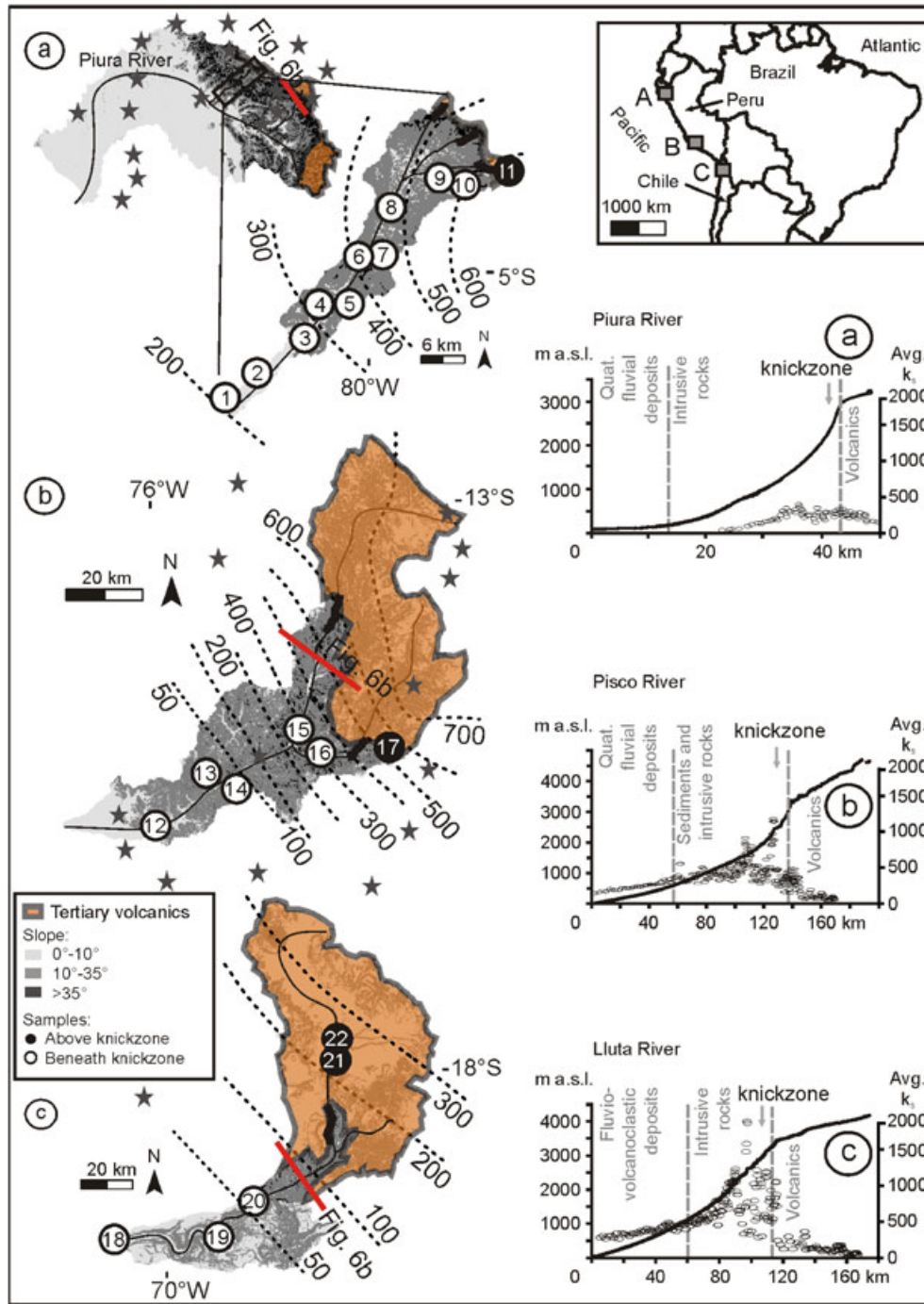


Figure 1. Hillslope inclination maps of the Rio Piura (a), Rio Pisco (b) and Rio Lluta (c) catchments. The knickzones are highlighted with a thick black line. Rain gauge locations are show with stars, along with isohets in mm yr^{-1} (Agteca, 2010). Also shown are sampling locations, river profiles (black line), channel steepness (k_s) values (black ovals) and the underlying lithologies (separated by dashed grey lines) along the longest flow path of each catchment.

knickzone tip are equivalent in the long term. A particular case of parallel retreat involves a resistant rock unit capping underlying weaker lithologies. Based on experimental studies, Gardner (1983) found that knickzones do not undergo parallel retreat where bedrock is homogenous, except where the substrate displays extensive and pervasive jointing. In this sense, a cap-rock must either exhibit higher erosional resistance than the underlying lithologies, or the underlying rocks must be heavily fractured. Here we explore the circumstances that have allowed the preservation of steep knickzones over 10^6 yr timescales in the Western Escarpment of the Andes using a combination of geologic maps, rock strength measurements and qualitative estimates of joint densities, topographic analyses, and ^{10}Be -derived denudation rates from three transverse

catchments that span 13° of latitude: the Rio Piura ($\sim 5^\circ\text{S}$), the Rio Pisco ($\sim 13^\circ\text{S}$) and the Rio Lluta ($\sim 18^\circ\text{S}$). We focus on the causal relationships implied by correlations between metrics representing climate forcing and topography across a region with a strong negative precipitation gradient from north to south and from east to west (Montgomery *et al.*, 2001). We propose that the maintenance of the Western Escarpment edge is the combined outcome of an episodic phase of surface uplift that separates the original stream into a lower steep segment and an upper low-gradient segment. In this case, the mechanism of headward retreat is controlled by the high incision rates related to high gradient channels in the steep knickzones relative to the shallower headwater reaches where incision rates have remained unaltered.

Setting

Geology

The Andean mountain belt forms a 9000 km long, north–south oriented range along the western edge of South America. The Andean orogen is located above the active subduction of the Farallón–Nazca plate beneath the South American plate. This subduction controlled arc magmatism since Jurassic times and uplift at 30 to 25 Ma ago (Isacks, 1988). In Peru and northern Chile, the river catchments draining the Western Escarpment are underlain by a suite of Quaternary sediments and low-grade metasediments of Mesozoic age (meta-sandstones, limestones, and graywackes) intruded by the Cretaceous to early Tertiary Coastal Batholith (granites and granodiorites). In the headwaters, these rocks are unconformably overlain by a hundreds of metres-thick series of Tertiary volcanoclastic deposits (Cobbing *et al.*, 1981; Fernández Dávila, 1993; García and Hérial, 2005) (Figure 1). As synthesized by Wipf (2006), the rock units underlying the volcanoclastic series have experienced four main phases of shortening and deformation since the Mesozoic: (i) the Early Cretaceous Mochica phase, involving large-scale folding of upper crustal rocks and magmatic intrusions of the Coastal Batholith (Megard *et al.*, 1984); (ii) the Late Cretaceous Peruvian phase (Jaillard *et al.*, 1996); (iii) the Tertiary Incaic phases involving folding and thrusting associated with exhumation of the Coastal Batholith and the deposition of widespread ignimbrite beds (McLaughlin, 1924; Steinmann, 1929); and (iv) the Quechua phase (Sebrier *et al.*, 1988). A key point to note is that the Tertiary ignimbrites experienced only the lattermost Quechua phase of deformation, which also drove the surface uplift that initiated gorge incision (Schildgen *et al.*, 2007; Jordan *et al.*, 2010). The underlying units were repeatedly subject to brittle-phase deformation and consequently are heavily fractured and foliated. A final phase of Quaternary uplift may be affecting the coastal regions of the catchments (Regard *et al.*, 2010).

Alluvial terraces are evident in the Western Escarpment downstream of the knickzones, where valleys widen to tens to hundreds of metres. In the Pisco valley (Steffen *et al.*, 2009), the valley floors are occupied by 5 to 60 m-thick sequences of Quaternary cut-and-fill terraces. These lower channel reaches, from the base of the knickzones to the coast, are also associated with loess cover but sparse to absent soil mantles. Within the knickzone reach, hillslopes are steepest (>35° in some locations) (Figure 1), and mixed bedrock–alluvial channels are deeply incised. Above the escarpment edge, streams exhibit low gradients, and soil-mantled hillslopes are gently sloping with convex forms, smooth curvatures, and sparse vegetation (Figure 2). Soils on the plateau are uniformly distributed and range from ~1 to 2 m thick, as evidenced by road cuts and gullies.

Climate

The Andean orogen has long influenced precipitation patterns in South America by providing a major topographic barrier to atmospheric circulation. Some time between 14 and 8 Ma, the rising Andean range had reached sufficient elevation to establish a rain shadow, leading to semiarid to hyperarid climate conditions on the western Central Andes (Hartley, 2003; Schlunegger *et al.*, 2010). In the subequatorial Andes between 3°S and 15°S, easterly trade winds during austral summer carry moisture from the Amazon basin to the headwaters of the study basins, whereas during winter, a persistent dry westerly wind hinders this easterly transfer of moisture (Garreaud *et al.*, 2003). In the subtropical belt of deserts (15°S–33°S), neither side of the

range receives much precipitation. The overall result is a strong negative precipitation gradient from the headwaters to the Pacific coast, coupled with decreasing moisture from north to south where the subequatorial north gives way to the semiarid central Andes (Figure 1).

Methods

¹⁰Be-derived denudation rates

We apply the basin-averaged cosmogenic nuclide method to catchments on the Western Escarpment (Brown *et al.*, 1995; Bierman and Steig, 1996; Granger *et al.*, 1996; Granger and Smith, 2000), and present new catchment-wide denudation rates from concentrations of *in situ*-produced cosmogenic ¹⁰Be in quartzose river sand from the Rio Pisco plus recalculated rates from the Rio Piura (Abbühl *et al.*, 2010) and Rio Lluta (Kober *et al.*, 2009). The integration time-scale varies with the rate of denudation, and may be calculated as the time taken to remove one absorption path length (i.e. ~0.6 m for rock; Lal, 1991). The denudation rates calculated here for Western Escarpment range from ~10 to 250 mm ky⁻¹, which corresponds to integration times as short as ~2.4 ka in the most rapidly eroding sections to more than 60 ka on the plateau. Hence, our results are not sensitive to short-term variations in surface erosion linked to human influences or recent climate fluctuations (von Blanckenburg, 2005; Vanacker *et al.*, 2007).

In the Pisco system, six samples were collected consecutively downstream along the main river and in transverse tributary channels (Figure 1 and Table I). The sample sites were selected to cover a range of geomorphologic domains including segments above and below the escarpment edge.

Laboratory methods

The grain size fraction from 0.4–1 mm was used for the quartz separation. For one sample from the Pisco catchment (Pis1.1), quartz was also extracted from the 0.25–0.4 mm size fraction to test for grain size effects on ¹⁰Be concentrations. While these two samples differ by greater than 2σ, Kober *et al.* (2009) found no significant differences in ¹⁰Be concentrations measured from different grain size fractions in the Lluta catchment. Since our samples indicate that there are potential grain size effects, we use only the 0.4–1 mm size fraction for the analysis in order to have an internally consistent dataset.

After sieving, magnetic grains were separated using a Frantz Magnetic Barrier Separator. A purified quartz mineral separate was produced by selective chemical dissolution using 5% hydrofluoric acid (after Kohl and Nishiizumi, 1992) repeated several times to remove any atmospheric ¹⁰Be. Beryllium was extracted from the dissolved quartz using ion exchange column separation (Aldahan and Possnert, 1998). The recovered Be-hydroxide was converted to BeO and mixed with Nb for accelerator mass spectrometry at the Tandem Laboratory, Uppsala University. The machine ¹⁰Be/⁹Be background was (4–6) × 10⁻¹⁵ and the blank ratio was (1–3) × 10⁻¹⁴. All measurements were normalized to the NIST SRM 4325 standard with a nominal ¹⁰Be/⁹Be ratio of 3.03 × 10⁻¹¹ (Nishiizumi *et al.*, 2007), based on a ¹⁰Be half-life of 1.51 ± 0.06 My (Hofmann *et al.*, 1987). For consistency, we have calculated all concentrations and denudation rates relative to the newer 1.39 ± 0.1 My ¹⁰Be half-life (Chmeleff *et al.*, 2010; Korschinek *et al.*, 2010). The use of either half-life in our denudation rate calculations yields results that are within measurement error of each other. Catchment specific shielding factors were calculated from 3D/

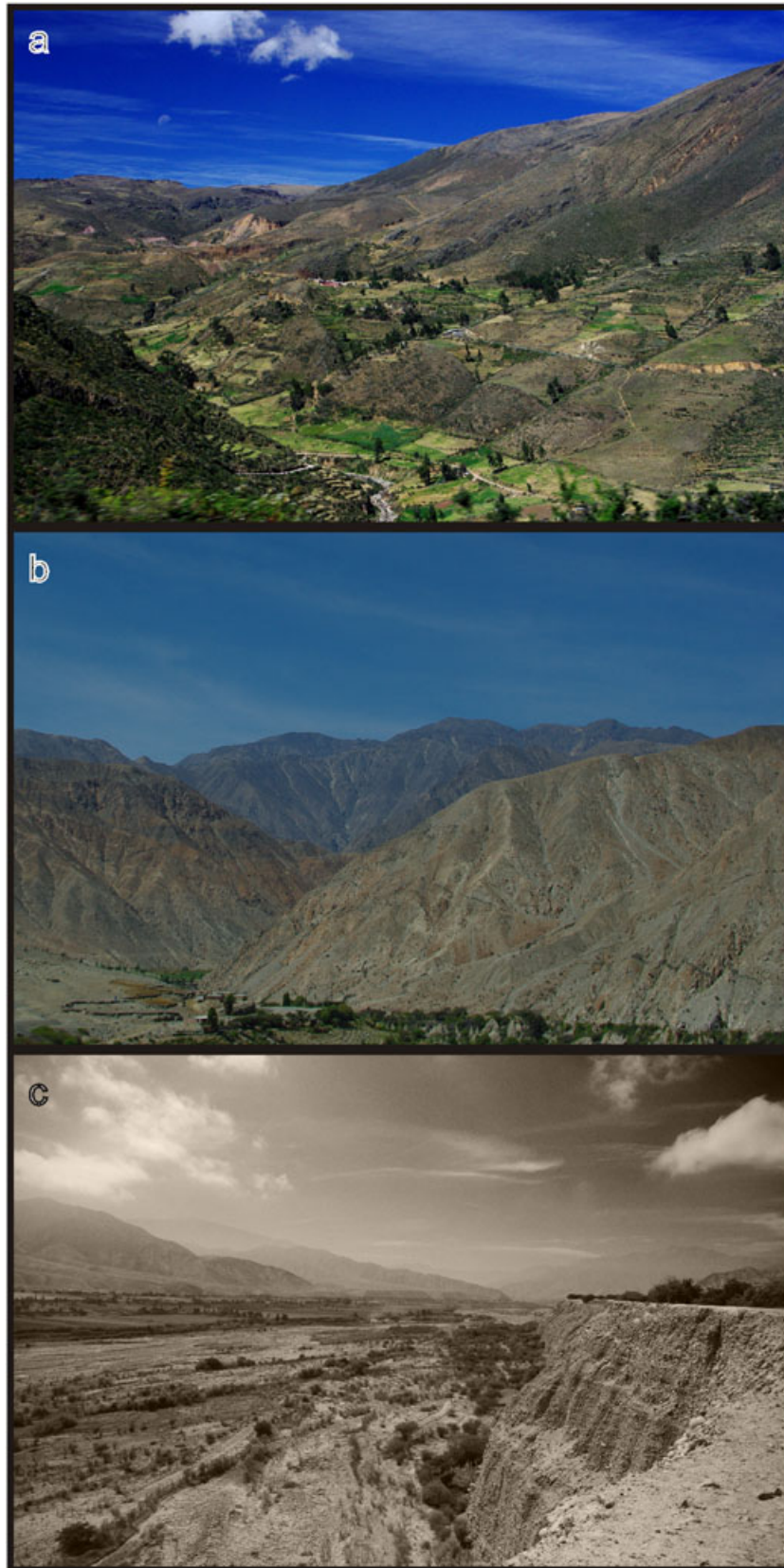


Figure 2. Landscapes of the Rio Pisco exemplifying (a) above, (b) within, and (c) below the knickzone on the Western Escarpment. This figure is available in colour online at wileyonlinelibrary.com/journal/espl

2D surface area ratios following Norton and Vanacker (2009) using the 90-m-resolution Shuttle Radar Topography Mission (SRTM) data. Total ^{10}Be production rates were calculated using a sea-level, high latitude ^{10}Be production rate of $5.1 \text{ atoms g}^{-1}_{\text{qtz}} \text{ yr}^{-1}$ scaled to altitude and latitude following Dunai (2000), and bedrock density was assumed to be 2.7 g cm^{-3} . No corrections for uplift or for paleomagnetic field variations were applied.

Morphometric properties

Relative rates of erosion are commonly inferred from morphometric properties including mean hillslope angle (Binnie *et al.*, 2007) and channel steepness (Safran *et al.*, 2005; Wobus *et al.*, 2006; Ouimet *et al.*, 2009). We extracted morphometric parameters from 90-m-resolution SRTM data and, as such, the

Table I. Cosmogenic nuclide data.

Sample	ID	Mean elevation ^a (m)	Longitude ^b (d.d.)	Latitude ^b (d.d.)	¹⁰ Be conc. ^c (x10 ⁴ atoms/gqtz/yr)	Shielding factor ^d	Production rate ^e (atoms/gqtz/yr)	Denudation rate ^f (mm/ky)	Total uncertainty ^g (%)	Apparent age ^f (kyr)
Piu6*	1	1418	-80.1583	-5.1041	7.92 ± 0.39	0.92	9.1	90.5 ± 6.5	10	9.5
Piu8*	2	1461	-80.1315	-5.0856	5.91 ± 0.53	0.91	9.4	125 ± 13	13	6.9
2_1*	3	468	-80.0738	-5.0427	6.21 ± 0.49	0.93	4.5	68.2 ± 5.7	11	14.7
Piu9*	4	1708	-80.0537	-5.0183	6.24 ± 0.52	0.91	11.1	135 ± 14	12	6.2
2_2*	5	1042	-80.0478	-5.0158	4.77 ± 0.49	0.89	7.0	118 ± 13	13	7.7
2_3*	6	1172	-80.0219	-4.9888	3.46 ± 0.48	0.83	7.7	165 ± 25	16	5.5
2_4*	7	1319	-80.0136	-4.9787	7.34 ± 0.71	0.88	8.5	88.4 ± 9.4	13	9.9
Piu10*	8	2054	-79.9960	-4.9451	7.32 ± 0.56	0.91	14.0	140 ± 15	13	5.8
Piu13*	9	2355	-79.9517	-4.9299	7.5 ± 1.5	0.88	17.1	156 ± 34	23	5.0
Piu12*	10	2147	-79.9466	-4.9257	5.84 ± 0.39	0.91	14.9	185 ± 19	13	4.3
Piu11*	11	3084	-79.8939	-4.9181	223.3 ± 5.4	0.99	26.8	8.08 ± 0.85	13	85.6
Pis11	12	3465	-75.8855	-13.7274	17.1 ± 1.2	0.92	33.5	131 ± 17	15	5.5
Pis5	13	1100	-75.7371	-13.6408	45.9 ± 2.3	0.92	7.2	11.63 ± 0.76	10	69.9
Pis1	14	3767	-75.7280	-13.6506	26.4 ± 1.8	0.93	39.7	100 ± 13	15	7.2
Pis1.1	-	3767	-75.7280	-13.6506	19.4 ± 1.6	0.93	39.7	136 ± 19	16	5.3
Pis9	15	4082	-75.5356	-13.5656	12.4 ± 1.9	0.93	47.2	251 ± 50	21	2.8
Pis4	16	4116	-75.3634	-13.5920	38.3 ± 2.3	0.95	48.1	84 ± 12	16	8.4
Pis2	17	4227	-75.2511	-13.5702	322 ± 11	0.98	51.0	10.3 ± 1.3	15	65.5
Ll3 ⁺	18	3487	-70.2833	-18.3833	72.1 ± 4.5	0.96	33.9	29.6 ± 3.7	15	24.0
Ll2 ⁺	19	3758	-70.0167	-18.4000	81.2 ± 3.3	0.96	39.5	30.3 ± 3.8	14	23.2
Ll1 ⁺	20	4063	-69.8667	-18.3333	89.0 ± 4.7	0.96	46.7	32.4 ± 4.3	15	21.5
Ll5 ⁺	21	4345	-69.6167	-17.9833	197 ± 12	0.98	54.3	16.8 ± 2.5	17	40.4
Ll4 ⁺	22	4323	-69.6167	-17.9833	203 ± 26	0.98	53.6	16.2 ± 2.9	19	42.1

^aMean basin elevation determined from SRTM 90m dataset.

^bSampling location.

^cNuclide concentrations for the Lluta catchments (Kober *et al.*, 2009) have been reduced by 1.096 to make them compatible with the new ¹⁰Be half-life of 1.39 Ma (Chmeleff *et al.*, 2010; Korschinek *et al.*, 2010).

^dTopographic shielding factors determined following Norton and Vanacker (2009) using the SRTM 90 m dataset.

^eProduction rates based on the scaling laws of Dunai (2000) and production formulas of Schaller *et al.* (2004).

^fDenudation rates and apparent ages calculated assuming cosmogenic steady state. The errors on denudation rates are analytical.

^gTotal (external) error for comparison with other methods.

*Concentrations from Abbühl *et al.*, 2010.

†Concentrations from Kober *et al.*, 2009.

Samples in grey are from the Meseta Plateau.

metrics determined here are smoothed with respect to the higher resolution DEMs used by Binnie *et al.* (2007) and DiBiase *et al.* (2010). Mean basin slope is calculated as the mean of all slope angles (derived from a 3 × 3 window) for each catchment. The steepness index of a channel, k_s , scales the relationship between channel gradient S and contributing drainage area, A (Flint, 1974) and is positively related to surface erosion rates in tectonically active areas (Safran *et al.*, 2005): $S = k_s A^{-\theta}$, where θ is the concavity index. We normalized channel steepness values (k_{sn}) to a standard reference concavity θ of 0.45 (Wobus *et al.*, 2006) for both the trunk streams and the entire watershed, using a 1000 m smoothing window, and 25 m contour sampling. The normalization of k_{sn} allows both inter-basin comparison (Korup, 2006) and the confirmation of knickzone locations along the river profiles (Figure 1). In an effort to identify how climate controls landscape morphology below the escarpment edge, three topographic sections across the drainage basins were extracted perpendicular to the trunk streams ~10 km downstream of their respective knickzones.

Contemporary precipitation rates in the field area are available from a variety of sources, but we utilize the Global Historical Climatology Network (GHCN) compilation (21 years average duration; see Agteca.org; Agteca, 2010) for its long and internally-consistent high-resolution records spanning all three study basins. The uncertainties reported in Table II for both the topographic metrics and precipitation data are taken from the intra-basin standard deviation; larger basins have

higher associated variance because they integrate over a wider range of topography and precipitation rates. The 1 σ error of the precipitation dataset is 180 mm yr⁻¹, and was determined by analyzing the inter-annual means at each station (total $n = 11204$). We note also that the precipitation patterns are similar to other data sets and differ only in the absolute magnitude, especially for the Rio Piura (Hydrological Atlas; Mettier *et al.*, 2009). Therefore, while the slope of the relationship between denudation rate and precipitation rate changes depending on the precipitation record, the trend remains the same.

Finally, bedrock strength was estimated using an N-type Schmidt Hammer on bedrock locally exposed in stream channels (for fresh bedrock), and on hillslopes (for weathered bedrock). For each rock type, 40 rebound values were measured at >10 cm intervals and errors were calculated as the 1 σ variance of each measurement set.

Results

As detailed above, precipitation decreases in both a N to S and E to W direction such that mean precipitation in the basins studied vary from ~650 to 20 mm yr⁻¹. Hillslope angles and channel steepness vary above and below the escarpment edge. The mean morphometric values, averaged for the area upstream of each ¹⁰Be sample, range from 5° to 29° for slope, and 6 m^{0.9}

Table II. Topographic and climatic data.

Sample	ID	Area ^a (km ²)	Altitude range ^b (km)	Slope ^c (deg.)	Relief ^d (m)	Normalized steepness index ^e (m ^{0.9})	Precipitation ^f (mm/yr)
Piu6*	1	191	0.1–3.4	18 ± 10	1038	154 ± 86	445 ± 97
Piu8*	2	185	0.1–3.4	19 ± 10	1067	159 ± 83	453 ± 91
2_1*	3	1.1	0.3–0.8	18 ± 7	640	±	311 ± 3
Piu9*	4	151	0.3–3.4	20 ± 10	1169	168 ± 83	486 ± 61
2_2*	5	11	0.4–1.8	23 ± 8	1205	150 ± 45	416 ± 26
2_3*	6	1.3	0.7–1.7	29 ± 7	1279	±	435 ± 6
2_4*	7	2.6	0.8–1.8	24 ± 7	1143	±	457 ± 8
Piu10*	8	98	1.0–3.4	20 ± 10	1193	157 ± 82	516 ± 48
Piu13*	9	7.1	1.6–3.1	23 ± 10	1231	152 ± 67	590 ± 23
Piu12*	10	3.4	1.6–2.9	21 ± 7	1409	108 ± 39	568 ± 11
Piu11*	11	1.1	3.0–3.1	5 ± 3	862	±	595 ± 7
Pis11	12	3642	0.4–5.3	18 ± 10	964	214 ± 226	453 ± 264
Pis5	13	0.2	0.9–1.2	19 ± 4	925	±	22 ± 1
Pis1	14	3084	0.7–5.3	18 ± 10	961	217 ± 240	526 ± 220
Pis1.1	-	3084	0.7–5.3	18 ± 10	961	217 ± 240	526 ± 220
Pis9	15	1844	1.3–5.3	17 ± 10	924	214 ± 266	593 ± 139
Pis4	16	671	2.4–5.0	15 ± 8	749	172 ± 174	652 ± 113
Pis2	17	17	3.8–4.5	11 ± 5	511	89 ± 46	647 ± 28
LI3 ⁺	18	3334	0.1–6.0	12 ± 9	655	145 ± 183	141 ± 66
LI2 ⁺	19	3020	0.7–6.0	12 ± 10	664	145 ± 188	153 ± 59
LI1 ⁺	20	2545	1.3–6.0	12 ± 10	647	140 ± 196	172 ± 41
LI5 ⁺	21	1324	3.6–6.0	9 ± 7	513	79 ± 53	204 ± 18
LI4 ⁺	22	881	3.6–6.0	8 ± 7	519	72 ± 49	205 ± 19

^aDrainage basin area upstream of sampling location.

^bMinimum and maximum basin elevation.

^cMean basin slope calculated using a 3 × 3 window from the 90m SRTM dataset.

^dMean local relief using a sliding circular window of 2.5 km radius.

^eMean channel steepness, k_{sn} , normalized to a concavity of 0.45 (Wobus *et al.*, 2006), including the 1 s.d. variance around the mean for each basin. It was not possible to obtain meaningful results for basins with areas less than 4 km².

^fMean basin precipitation rate derived from the GHCN data (Agteca, 2010), including the 1 s.d. variance around the mean for each basin. 1 σ error for the entire dataset is 180 mm/yr.

Samples in grey are from the Meseta Plateau.

to 217 m^{0.9} for normalized channel steepness (Table II). Denudation rates in the catchments vary from ~8 to 185 mm ky⁻¹ in the Piura, ~10 to 250 mm ky⁻¹ in the Pisco, and ~15 to 29 mm ky⁻¹ in the Lluta. Upstream from the knickzones and the escarpment edge, denudation rates are less than 15 mm ky⁻¹ in all catchments.

The measured denudation rates plot into two distinct groups with respect to precipitation rates (Figure 3). Denudation rates are rapid below the escarpment edge where modern precipitation is high, whereas plateau denudation rates are relatively slow irrespective of precipitation.

Denudation rates and the variance in denudation rates both increase with steeper mean basin slopes and channel steepness (Figure 4). However, given the distinctive relationship that exists between rates of denudation and precipitation on the Meseta/Altiplano (Figure 3), we treat the plateau data separately from those below the escarpment edge. Consequently, correlations between denudation rate and mean basin slope and channel steepness become considerably weaker when the plateau data are excluded ($R^2 = 0.37$ and 0.10 , respectively). Despite being weak, the correlation between denudation rate and mean basin slope is significant, $P < 0.05$. On the Meseta/Altiplano, denudation rates, mean basin slopes, and channel steepness all remain constantly low and do not depend on precipitation rate.

In each of the study catchments, the high-elevation plateau comprises Tertiary ignimbrites and volcanoclastic units, whereas the knickzones are incised into the underlying highly-fractured Cretaceous intrusives and the folded and jointed Jurassic meta-sediments. Visual inspection of the Tertiary volcanic cap-rocks reveals fracture and joint spacing that generally exceeds one

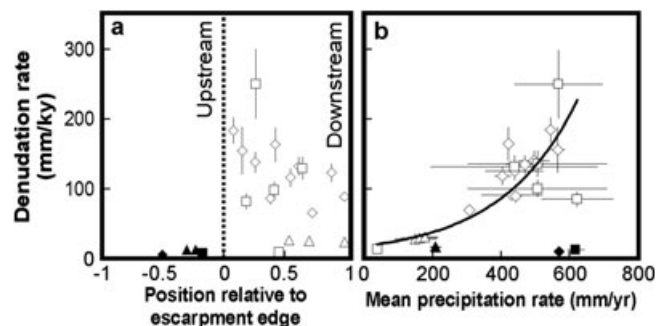


Figure 3. (a) Basin-averaged denudation rates of the Piura (diamonds), Pisco (squares) and Lluta (triangles) river catchments relative to the edge of the Meseta plateau (negative values are upstream from the knickzone and positive values downstream). Samples from below the escarpment are indicated by open symbols, and black symbols indicate samples from the Meseta/Altiplano. (b) Mean annual precipitation plotted against basin-averaged denudation rates. An exponential curve fits the data with an $R^2 = 0.82$; $P < 0.05$.

decimetre, whereas the strongly fractured and foliated Mesozoic rocks are typically more closely jointed in the sub-decimetre range (Figure 5a, b). Schmidt Hammer rebound values show that fresh outcrops are stronger than weathered rocks in terms of point-specific rock strength; however, the lack of any significant differences between the plateau and knickzone rocks suggests that fracture and joint spacing are the main determinants of substrate erodibility (Figure 5c).

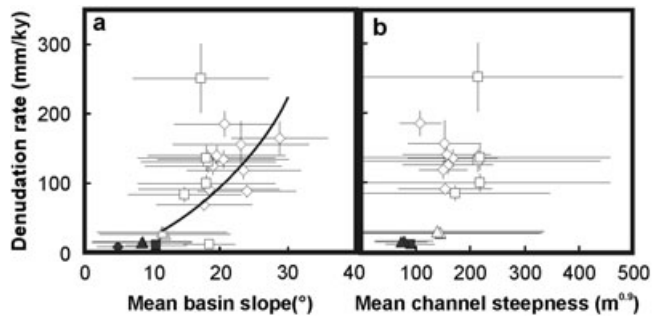


Figure 4. Cosmogenic nuclide-derived denudation rates (Piura (diamonds), Pisco (squares) and Lluta (triangles)) (mean values ± 1 standard deviation) plotted against (a) mean catchment hillslope angle (power law, $R^2=0.37$, $P<0.05$) and (b) mean channel steepness (power law, $R^2=0.10$, $P>0.05$) (see Table II). Note that some samples do not appear in Figure 4b because catchment areas $<4\text{ km}^2$ failed to yield valid channel steepness values (Table II). Samples from below the escarpment are indicated by open symbols, and black symbols indicate samples from the Meseta/Altiplano.

The distribution of hillslopes in the three catchments varies considerably (Figure 6a). The Lluta is dominated by low slope angles, whereas the Pisco and Piura show progressive steepening. Valley cross-sections through the knickzones in each catchment also show distinct differences in hillslope morphology (Figure 6b). The Lluta valley in northern Chile, with the lowest precipitation and denudation rates, has a well-formed plateau, and a $\sim 10\text{ km}$ wide valley that displays little dissection by tributary valleys. To the north, the wetter and more rapidly denuding Pisco and Piura catchments have incised valleys that are $>20\text{ km}$ wide, accompanied by multiple, deeply dissected tributaries.

Discussion

The Meseta/Altiplano cap-rocks

In each of the three study catchments, the Meseta/Altiplano is underlain by Tertiary ignimbrites and volcanoclastic units, which we suggest function as cap-rocks that help to maintain the steep slopes below the escarpment edge during knickpoint retreat. This is justified by two arguments. First, the escarpment edge in these basins is defined by a lithological contact that we interpret to indicate a change in rock mass strength. Our Schmidt hammer tests do not reveal any significant differences in point-specific rock strength above and below the escarpment edge (Figure 5c). However, based on the boulder-sized bed materials ($\leq 1\text{ m}$), and the prevalence of plucked joint-planes along the knickzones (Figure 5b), we argue that fluvial plucking is the dominant erosional process, and hence fracture and joint spacing are the main determinants of substrate erodibility (Whipple, 2004). Second, the cap-rocks impose a control on fluvial incision rates by influencing channel gradients across the Meseta/Altiplano. The slow denudation of the plateau reflects the gently sloping, low-relief terrain that is geomorphologically decoupled from the rapidly eroding knickzone reaches downstream (Figure 4).

Figure 5. (a) Joint spacing in the ignimbrites and volcanoclastics on the plateau are decimetre to metre scale. (b) Jointing in the metasediments and granitoid rocks below the escarpment display sub-decimetre scale jointing. (c) Schmidt Hammer rebound values for weathered and fresh volcanic and granitic lithologies overlap within 1σ error. This figure is available in colour online at wileyonlinelibrary.com/journal/espl

Uplift and development of parallel knickpoint retreat

Much of the Meseta/Altiplano is unaffected by the Late Miocene phase of uplift, since the streams crossing it remain graded to the



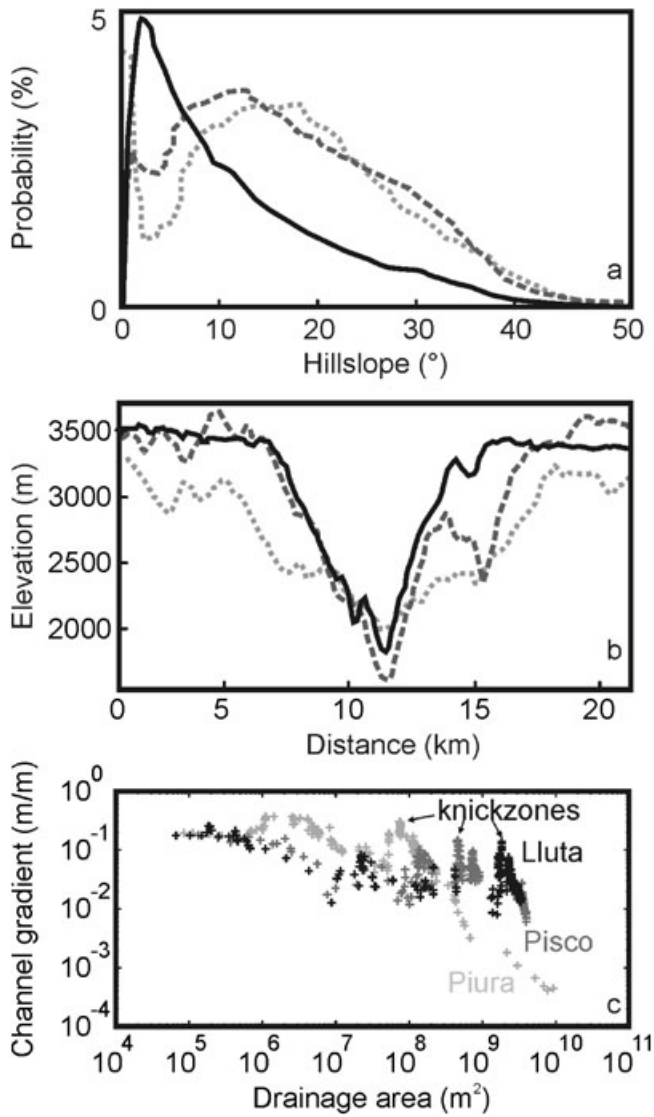


Figure 6. (a) Slope distributions for the Rio Piura (dotted), Rio Pisco (dashed), and Rio Lluta (solid) catchments. (b) Topographic cross-sections through the knickzone of each of the three study catchments. (c) log(slope)–log(area) plots for the three rivers showing the locations of the prominent knickzones.

pre-uplift base level (Kober *et al.*, 2006; Schlunegger *et al.*, 2006; Schildgen *et al.*, 2007). We envisage that surface uplift between 7.5 and 10 Ma (García and Hérail, 2005; von Rotz *et al.*, 2005; Schildgen *et al.*, 2007) created a steepening ramp that promoted stripping of the Tertiary cap-rocks in the west and knickpoint retreat into the underlying fractured Cretaceous intrusives and Jurassic meta-sedimentary rocks. Knickzones continue to propagate headward via parallel retreat thanks to the presence of the Tertiary cap-rocks forming the Meseta/Altiplano. The differential erodibility at the escarpment edge helps to maintain steep slopes and impedes propagation of the base level signal that would otherwise lead to channels steepening upstream of the knickzones. Renewed Quaternary uplift (Jordan *et al.*, 2010; Regard *et al.*, 2010) may also be affecting these streams. In particular, the Lluta River is steeper near the coast than would be expected for a graded stream (Figures 1 and 6c).

Spatial differences in how climate affects denudation rates

On the Meseta/Altiplano above the escarpment edge, denudation rates remain uniformly low irrespective of precipitation

rates (Figure 3). This plateau landscape, characterized by smooth, convex hillslopes, shows no evidence for a tectonic forcing (i.e. faults that offset dated deposits) over the past several millions of years (Zeilinger *et al.*, 2005; Hoke *et al.*, 2007). Our data thus supports the arguments of Ahnert (1970) and data of von Blanckenburg *et al.* (2004) that in the absence of relative base-level fall denudation rates do not necessarily increase with higher precipitation rates.

Denudation rates below the escarpment edge are generally an order of magnitude faster than those on the plateau and scale with precipitation (Figure 3). We interpret this to indicate that the knickzones in the studied rivers are eroding into the escarpment edge at a rate that is proportional to stream power; that is, some function of the product of channel gradient and discharge. Given that precipitation controls river discharge, this interpretation implicates climate as an important control on erosion beyond the plateau edge. Accordingly, we attribute to discharge (via precipitation) the notable differences in cross-valley hillslope morphology (Figure 6).

Links between topography and denudation rates

Steep mountain rivers serve as the local base level for hillslope erosion, though ongoing fluvial incision rapidly brings hillslopes to a condition of maximum steepness, determined by rock-mass strength, above which mass failure is likely (Schmidt and Montgomery, 1995). We interpret the poor scaling between mean basin slope and denudation rates (Figure 4a) as indicating that hillslopes below the escarpment are close to threshold values; that is, the hillslopes are near the limit of diffusive creep (Roering *et al.*, 1999; Montgomery and Brandon, 2002; Binnie *et al.*, 2007). Field work (Schneider *et al.*, 2008) and satellite imagery confirm the presence of shallow landsliding and abundant debris flow channels in the region around the knickzone. The change in jointing density near the escarpment edge may contribute to the preservation of steep slopes without any impact from precipitation.

Rather than scaling with denudation rates, channel steepness values appear to cluster around $200 \text{ m}^{0.9}$ (Figure 4b). Using an expanded dataset for northern Peru, Abbühl *et al.* (2010) found a stronger correlation between channel steepness and denudation rates for values $\leq 200 \text{ m}^{0.9}$. A non-linear and weak correlation between denudation rates and channel steepness reported by Ouimet *et al.* (2009) for three rivers draining the Tibet plateau was interpreted as being due to the combined effects of critical thresholds involved in sediment transport coupled with the typically large variability in river discharge. We suspect that sediment entrainment thresholds may be similarly implicated in our study basins, given the large flood variabilities documented for northern Peru during El Niño events (Mettier *et al.*, 2009). This further implies that for settings in which precipitation is highly variable, both in time and space, the mean basin hillslope may reflect denudation rates more faithfully than channel steepness metrics.

Can El Niño events be detected in landscape morphology?

The effects of El Niño precipitation events on ¹⁰Be based denudation rates and channel morphologies were recently investigated by Abbühl *et al.* (2010). According to these authors, channels exhibit higher concavities where the downstream increase in water discharge related to El Niño events is highest. As described by Zaprowski *et al.* (2005) transient changes in precipitation rate manifest as increased

channel concavity due to increased stream power. Upstream of these highly concave stream segments, with an upper boundary of ~1500 m.a.s.l. (Mettier *et al.*, 2009), channels appear not to have been modified by El Niño precipitation perturbations. Hence, considering that the escarpment edge is at ~3000 m.a.s.l., we infer that El Niño events have not influenced the pattern of headward retreat or the shape of the escarpment edge. El Niño events decrease in magnitude towards the south from Piura in northern Peru to Lluta in northern Chile (McPhaden, 1999), and even in the Rio Piura, where El Niño precipitation is strongest (Mettier *et al.*, 2009), its effects are significant only at the hillslope scale in the lower channel reaches (Abbühl *et al.*, 2010).

Conclusions

We show that in the Western Escarpment of the northern and central Andes (northern Peru to northern Chile), parallel knickpoint retreat has been assisted by the presence of cap rock with relatively low fracture density that maintains steep slopes at the escarpment edge. ^{10}Be concentrations in fluvial sediment suggest that climate exerts significant control on denudation rates and hillslope morphology in the deeply dissected terrain below the escarpment, but not on the Meseta/Altiplano where denudation rates remain essentially constant across a 4-fold range in annual precipitation. Conversely, below the escarpment, the same 4-fold range in precipitation drives a 10-fold variation in denudation rates.

Initiated by tectonic perturbation in the Late Miocene, the subsequent development of spatial differences in hillslope morphology strongly implicates climate-driven erosional processes across the deeply incised terrain below the escarpment edge: valley width and the extent of dissection both appear to increase with increasing annual precipitation to the north. The distributions of morphology and denudation rates are the combined outcomes of climate and differential substrate erodibility as knickzones have propagated headward into the plateau.

Acknowledgements—We thank H. Schneider, D. Steffen, and K. Ramseyer for their help in the field, D. Rieke-Zapp for ArcGIS help, and T. Schildgen for improving an earlier version of the manuscript. This research was supported by the Swiss National Science Foundation (grant no. 200020-121680/1).

References

- Abbühl L, Norton KP, Schlunegger F, Kracht O, Aldahan A, Possnert G. 2010. El Niño forcing on ^{10}Be -based surface denudation rates in the northwestern Peruvian Andes? *Geomorphology* **123**: 257–268. doi: 10.1016/j.geomorph.2010.07.017.
- Agteca. 2010. Global Historical Climatology Network (GHCN-Monthly database) compilation for Peru by T.A. Cochrane. Downloaded July 2010 from Agteca.org (<http://www.agteca.org/climate.htm>)
- Ahnert F. Functional relationship between denudation, relief, and uplift in large mid-latitude drainage basins. *American Journal of Science* **268**: 243–263.
- Aldahan A, Possnert G. 1998. A high-resolution ^{10}Be profile from deep sea sediment covering the last 70 ka: indication for globally synchronized environmental events. *Quaternary Science Reviews* **17**: 1023–1032.
- Bierman P, Steig EJ. 1996. Estimating rates of denudation using cosmogenic isotope abundances in sediment. *Earth Surface Processes and Landforms* **21**: 125–139. doi: 10.1002/(SICI)1096-9837(199602)21:2<125::AID-ESP511>3.0.CO;2-8.
- Binnie SA, Phillips WM, Summerfield MA, Fitfield LK. 2007. Tectonic uplift, threshold hillslopes, and denudation rates in a developing mountain range. *Geology* **35**: 743–746. doi: 10.1130/G23641A.1.
- Brown ET, Stallard RF, Larsen MC, Raisbeck GM, Yiu F. 1995. Denudation rates determined from the accumulation of in situ-produced ^{10}Be in the Luquillo Experimental Forest, Puerto Rico. *Earth and Planetary Science Letters* **129**: 193–202.
- Cobbing EJ, Pitcher WS, Wilson JJ, Baldock JW, Taylor WP, McCourt WJ, Snelling N. 1981. *The Geology of the Western Cordillera of Northern Perú*. Institute of Geological Sciences Overseas, Memoirs 5: London.
- Chmeleff J, von Blanckenburg F, Kossert K, Jakob D. 2010. Determination of the ^{10}Be half-life by multicollector ICP-MS and liquid scintillation counting. *Nuclear Instruments and Methods in Physics Research B* **268**: 192–199.
- DiBiase RA, Whipple KX, Heimsath AM, Quimet WB. 2010. Landscape form and millennial erosion rates in the San Gabriel Mountains, CA. *Earth and Planetary Science Letters* **289**: 134–144. doi:10.1016/j.epsl.2009.10.036.
- Dunai TJ. 2000. Scaling factors for production rates of in-situ produced cosmogenic nuclides: a critical reevaluation. *Earth and Planetary Science Letters* **176**: 157–169.
- Fariás M, Charrier R, Carretier S, Martinod J, Fock A, Campbell D, Cáceres J, Comte D. 2008. Late Miocene high and rapid surface uplift and its erosional response in the Andes of central Chile (33°–35°S). *Tectonics* **27**: TC1005. doi:10.1029/2006TC002046.
- Fernández Dávila M. 1993. Geología de los cuadrángulos de Pisco, Guadalupe, Punta.
- Flint JJ. 1974. Stream gradient as a function of order, magnitude, and discharge. *Water Resources Research* **10**: 969–973.
- García M, Hérail G. 2005. Fault-related folding, drainage network evolution and valley incision during the Neogene in the Andean Precordillera of Northern Chile. *Geomorphology* **65**: 279–300. doi: 10.1016/j.geomorph.2004.09.007.
- Gardner TW. 1983. Experimental study of knickpoint and longitudinal profile evolution in cohesive, homogeneous material. *Geological Society of America Bulletin* **94**: 664–672. doi: 10.1130/0016-7606(1983)94<664:ESOKAL>2.0.CO;2.
- Garreaud R, Vuille M, Clement AC. 2003. The climate of the Altiplano: observed current conditions and mechanisms of past changes. *Palaeogeography, Palaeoclimatology, Palaeoecology* **194**: 5–22. doi: 10.1016/S0031-0182(03)00269-4.
- Granger DE, Smith AL. 2000. Dating buried sediments using radioactive decay and muogenic production of ^{26}Al and ^{10}Be . *Nuclear Instruments and Methods in Physics Research B* **172**: 822–826.
- Granger DE, Kirchner JW, Finkel R. 1996. Spatially averaged long-term erosion rates measured from in situ-produced cosmogenic nuclides in alluvial sediment. *Journal of Geology* **104**: 249–257.
- Hartley AJ. 2003. Andean uplift and climate change. *Journal of the Geological Society of London* **160**: 7–10. doi: 10.1144/0016-764902-083.
- Hofmann HJ, Beer J, Bonani G, Von Gunten HR, Raman S, Suter M, Walker RL, Wolfli W, Zimmermann D. 1987. ^{10}Be : half-life and AMS standards. *Nuclear Instruments and Methods in Physics Research B* **29**: 32–36.
- Hoke GD, Isacks BL, Jordan TE, Blanco N, Tomlinson AJ, Ramezani J. 2007. Geomorphic evidence for post-10 Ma uplift of the western flank of the central Andes 18°30'–22°S. *Tectonics* **26**: TC5021. doi: 10.1029/2006TC002082.
- Isacks BL. 1988. Uplift of the Central Andean Plateau and bending of the Bolivian Orocline. *Journal of Geophysical Research* **93**: 3211–3231. doi: 10.1029/JB093iB04p03211.
- Jaillard E, Soler P. 1996. Cretaceous to early Paleogene tectonic evolution of the northern Central Andes (0–18 degrees S) and its relations to geodynamics. *Tectonophysics* **259**: 41–53.
- Jordan TE, Nester PL, Blanco N, Hoke GD, Davila F, Tomlinson AJ. 2010. Uplift of the Altiplano-Puna plateau: a view from the west. *Tectonics* **29**: TC5007. doi:10.1029/2010TC002661.
- Kober F, Schlunegger F, Zeilinger G, Schneider H. 2006. Surface uplift and climate change: the geomorphic evolution of the Western Escarpment of the Andes of northern Chile between the Miocene and present. In *Tectonics, Climate, and Landscape Evolution*, Willett SD, Hovius N, Brandon MT, Fisher DM (eds). Geological Society of America Special Paper **398**: 75–86.
- Kober F, Ivy-Ochs S, Zeilinger G, Schlunegger F, Kubik PW, Baur H, Wieler R. 2009. Complex multiple cosmogenic nuclide concentration and histories in the arid Rio Lluta catchment, northern Chile. *Earth Surface Processes and Landforms* **34**: 398–412. doi: 10.1002/esp.1748.
- Kohl CP, Nishiizumi K. 1992. Chemical isolation of quartz for measurement of in situ-produced cosmogenic nuclides. *Geochimica et Cosmochimica Acta* **56**: 3583–3587.

- Korschinek G, Bergmaier A, Faestermann T, Gertmann UC, Knie K, Rugel G, Wallner A, Dillmann I, Dollinger G, Lierse von Gosstowski Ch, Kossert K, Maiti M, Poutivtsev M, Rimmert A. 2010. A new value for the ^{10}Be half-life by heavy-ion elastic recoil detection and liquid scintillation counting. *Nuclear Instruments and Methods in Physics Research B* **268**: 187–191.
- Korup O. 2006. Rock-slope failure and the river long profile. *Geology* **34**: 45–48.
- Lal D. 1991. Cosmic ray labeling of erosion surfaces: in situ nuclide production rates and erosion models. *Earth and Planetary Science Letters* **104**: 424–439. doi: 10.1016/0012-821X(91)90220-C.
- McLaughlin DH. 1924. Geology and physiography of the Peruvian cordillera, Departments of Junin and Lima. *Geological Society of America Bulletin* **35**: 591–632.
- McPhaden MJ. 1999. Genesis and evolution of the 1997–98 El Niño. *Science* **283**: 950–954.
- Megard F, Noble DC, Mckee EH, Bellon H. 1984. Multiple pulses of Neogene compressive deformation in the Ayacucho Intermontane Basin, Andes of Central Peru. *Geological Society of America Bulletin* **95**: 1108–1117.
- Mettier R, Schlunegger F, Schneider H, Rieke-Zapp D, Schwab M. 2009. Relationships between landscape morphology, climate and surface erosion in northern Peru at 5°S latitude. *International Journal of Earth Science* **98**: 2009–2022. doi: 10.1007/s00531-008-0355-7.
- Montgomery DR, Brandon MT. 2002. Topographic controls on erosion rates in tectonically active mountain ranges. *Earth and Planetary Science Letters* **201**: 481–489. doi: 10.1016/S0012-821X(02)00725-2.
- Montgomery RD, Balco G, Willett SD. 2001. Climate, tectonics, and the morphology of the Andes. *Geology* **29**: 579–582.
- Nishiizumi K, Imamura M, Caffee M, Southon J, Finkel R, McAnich J. 2007. Absolute calibration of Be-10 AMS standards. *Nuclear Instruments and Methods in Physics Research B* **258**: 403–413.
- Norton KP, Vanacker V. 2009. Effects of terrain smoothing on topographic shielding correction factors for cosmogenic nuclide-derived estimates of basin-averaged denudation rates. *Earth Surface Processes and Landforms* **34**: 145–154. doi: 10.1002/esp.1700.
- Ouimet WB, Whipple KX, Granger DE. 2009. Beyond threshold hillslopes: channel adjustment to base-level fall in tectonically active mountain ranges. *Geology* **37**: 579–582. doi: 10.1130/G30013A.1.
- Regard V, Saillard M, Martinod J, Audin L, Carretier S, Pedoja K, Riquelme R, Paredes P, Hérail G. 2010. Renewed uplift of the Central Andes Forearc revealed by coastal evolution during the Quaternary. *Earth and Planetary Science Letters* **297**: 199–210. doi:10.1016/j.epsl.2010.06.020
- Roering J, Kirchner JW, Dietrich W. 1999. Evidence for nonlinear, diffusive sediment transport on hillslopes and implications for landscape morphology. *Water Resources Research* **35**: 853–870.
- Safran EB, Bierman PR, Aalto R, Dunne T, Whipple KX, Caffee M. 2005. Erosion rates driven by channel network incision in the Bolivian Andes. *Earth Surface Processes and Landforms* **30**: 1007–1024. doi: 10.1002/esp.1259.
- Schildgen TF, Hodges KV, Whipple KX, Reiners PW, Pringle MS. 2007. Uplift of the western margin of the Andean plateau revealed from canyon incision history, southern Peru. *Geology* **35**: 523–526. doi: 10.1130/G23532A.1.
- Schildgen TF, Balco G, Shuster DL. 2010. Canyon incision and knickpoint propagation recorded by apatite $^4\text{He}/^3\text{He}$ thermochronometry. *Earth and Planetary Science Letters* **293**: 377–387. doi: 10.1016/j.epsl.2010.03.009.
- Schlunegger F, Zeilinger G, Kounov A, Kober F, Hüsler B. 2006. Scale of relief growth in the forearc of the Andes of Northern Chile (Arica latitude, 18° S). *Terra Nova* **18**: 217–223. doi: 10.1111/j.1365-3121.2006.00682.x.
- Schlunegger F, Kober F, Zeilinger G, von Rotz R. 2010. Sedimentology-based reconstructions of paleoclimate changes in the Central Andes in response to the uplift of the Andes, Arica region between 19 and 21°S latitude, northern Chile. *International Journal of Earth Science* **99**: 123–137. doi: 10.1007/s00531-010-0572-8.
- Schmidt KM, Montgomery DR. 1995. Limits to relief. *Science* **270**: 617–620.
- Schneider H, Schlunegger F, Schwab M. 2008. Channelized and hillslope sediment transport and the geomorphology of mountain belts. *International Journal of Earth Sciences* **97**: 179–192.
- Sebrier M, Lavenue A, Fornari M, Soulas JP. 1988. Tectonics and uplift in Central Andes (Peru, Bolivia, and Northern Chile) from Eocene to Present. *Géodynamique* **3**: 85–106.
- Steffen D, Schlunegger F, Preusser F. 2009. Drainage basin response to climate change in the Pisco valley, Peru. *Geology* **37**: 491–494. doi: 10.1130/G25475A.1.
- Steinmann G. 1929. *Geologie von Peru-Heidelberg*. Carl Winters Universitätsbuchhandlung.
- Thouret J-C, Wörner G, Gunnell Y, Singer B, Zhang X, Souriot T. 2007. Geochronologic and stratigraphic constraints on canyon incision and Miocene uplift of the Central Andes in Peru. *Earth and Planetary Science Letters* **263**: 151–166. doi: 10.1016/j.epsl.2007.07.023.
- Vanacker V, von Blanckenburg F, Govers G, Molina A, Poesen J, Deckers J, Kubik P. 2007. Restoring dense vegetation can slow mountain erosion to near natural benchmark levels. *Geology* **35**: 303–306. doi: 10.1130/G23109A.
- von Blanckenburg F. 2005. The control mechanisms of erosion and weathering at basin scale from cosmogenic nuclides in river sediment. *Earth and Planetary Science Letters* **237**: 462–479. doi: 10.1016/j.epsl.2005.06.030.
- von Blanckenburg F, Hewawasam T, Kubik PW. 2004. Cosmogenic nuclide evidence for low weathering and denudation in the wet, tropical highlands of Sri Lanka. *Journal of Geophysical Research* **109**: doi: 10.1029/2003JF000049.
- von Rotz R, Schlunegger F, Heller F, Villa I. 2005. Assessing the age of relief growth in the Andes of northern Chile: magneto-polarity chronologies from Neogene continental sections. *Terra Nova* **17**: 462–471. doi: 10.1111/j.1365-3121.2005.00634.x.
- Whipple KX. 2004. Bedrock rivers and the geomorphology of active orogens. *Annual Reviews in Earth and Planetary Science Letters*. **32**: 151–185.
- Wipf MA. 2006. Evolution of the Western Cordillera and coastal margin of Peru: evidence from low-temperature thermochronology and geomorphology. PhD thesis ETH. 16383, 152 p. doi:10.3929/ethz-a-005146374.
- Wobus C, Whipple KX, Kirby E, Snyder E, Johnson J, Spyropoulos K, Crosby B, Sheehan D. 2006. Tectonics from topography: procedures, promise, and pitfalls. In *Tectonics, Climate, and Landscape Evolution*, Willett SD, Hovius N, Brandon MT, Fisher DM. (eds). Geological Society of America Special Paper **398**: 55–74.
- Zaprowski B, Pazzaglia FJ, Evenson EB. 2005. Influences on profile concavity and river incision. *Journal of Geophysical Research, Earth Surface* **110**: F03004, doi:10.1029/2004JF000138.
- Zeilinger G, Schlunegger F, Simpson G. 2005. The Oxaya anticline (northern Chile): a buckle enhanced by river incision? *Terra Nova* **17**: 368–375. doi: 10.1111/j.1365-3121.2005.00622.x.